

# A novel slack enabling tendon drive that improves efficiency, size, and safety in soft wearable robots

Hyunki In, Useok Jeong, Haemin Lee, and Kyu-Jin Cho, *Member, IEEE*

**Abstract**—Tendon drives are widely used in robotics. The compliance of the tendon in such drives suits them for soft robots, including soft wearable robots, but several issues impede their use. Generally, the tendon should always maintain tension to prevent derailment from the spool. However, in soft robots, tendon tension induces high friction forces owing to the absence of ball bearings. Because the kinematics of the soft robot is basically nonlinear and changed by the deformation of the structure, the kinematic difference between the soft structure and the spool causes derailment of the tendon. Moreover, continuously maintained tension in soft wearable robots causes safety issues. The linear actuator can be an option. However, the need to increase the length of the linear actuator to accommodate the excursion length of its tendon is a barrier to its use in small-scale applications. To preclude this issue, a slack-enabling actuator that employs a spool is proposed. The space efficiency of the spool enables the mechanism to be small, and a one-way clutch applies unidirectional friction force to the tendon to tighten the tendon around the spool. This paper describes the design concept for the slack-enabling mechanism, its design optimization, and system identification for force control.

**Index Terms**—Actuator, Slack enabling mechanism, Soft robot, Soft wearable robot, Tendon drive.

## I. INTRODUCTION

Soft robots and rigid robots have different requirements for actuators. Because soft robots perform adaptable motions with their soft body, their actuators should be made of soft components if the actuator is embedded internally. For compact system, many soft robots have embedded actuators such as shape memory alloy [1], electroactive polymer [2], and bi-stable actuators [3]. However, up to now, the force and motion abilities of embedded actuators have been limited. To overcome these limitations, using a soft transmission to transmit the power of an external actuator has been tried. The great advantage of the external actuator is that it allows minimization of the end effector by externally locating the large

This research was supported by the Basic Science Research program through the National Research Foundation of Korea (NRF) funded by the Ministry of Science, ICT & Future Planning (2015M3C1B2052817).

Hyunki In is with Korea institute of industrial technology (e-mail: inhk@kitech.re.kr, phone:82-63-920-1289).

The other authors are with the Biorobotics Laboratory, School of Mechanical & Aerospace Engineering/IAMD, Seoul National University, Seoul, Republic of Korea (e-mail: Kyu-jin Cho, kjcho@snu.ac.kr, phone: 82-2-880-1663, fax: 82-2-880-1663).

actuator. Moreover, with its compliant transmission, the end effector remains soft, even though the external actuator is rigid (e.g., pneumatics [4] and tendons [5]).

Several studies describe wearable robots built from soft materials and soft structures [6]–[13], which allow the system to be compact. We will call such a device a “soft wearable robot.” Soft wearable robots employ various kinds of actuation systems, including pneumatic actuators [6], leaf springs [7], shape memory alloy [8] and tendon drives [9]–[13]. Often the actuator of a wearable robot must be located externally to decrease the inertia and weight of the body part. In a tendon drive system, the actuator can be located away from the part that is worn by using a Bowden cable.

Cho *et al.* developed a soft tendon routing system to apply a tendon drive to a soft wearable robot [13]. Soft tendon routing consists of soft structures such as tubes made of soft materials. The tendon path is closed to prevent derailment of the tendon from the path.

One issue with soft tendon routing is pre-tension of the tendons. In soft wearable robots, pre-tension can cause discomfort or injury, as well as decreased efficiency. To reduce or eliminate the pre-tension problem, the tendon needs to be fully released or even pushed by the actuator when the actuator releases it, but slackening occurs when tension is decreased. If a spool is used to drive the tendon, slackening may cause the tendon to derail from the spool, resulting in system failure.

Several solutions have been proposed to prevent this derailing. Walsh *et al.* attempted to encase the spool to prevent tendon derailment [14]. However, they found that the tendons sometimes jammed between the spool and the case in spite of the careful provision of a gap between the spool and the case. Mao and Agrawal [15] placed a rubber piece in front of the spool. The rubber piece continuously applies the friction force to the tendon. Then the tension of the wire around the spool is maintained while the tendon is wound by the spool. Chernyak *et al.* [16] used an active tensioner to keep the cable from derailing by pulling tendon when the tension is decreased. However, none of these mechanisms eliminates tension on the tendon when it is released.

Another solution is to eliminate the spool by utilizing linear actuators [17]. Linear actuators do not fail even if slackening occurs. However, linear actuators have a disadvantage in terms of their size because they must be longer than the required stroke of the tendon.

In this paper we propose a novel slack enabling mechanism that employs a tendon drive using a spool. A slack enabling mechanism mechanically maintains tension around a spool regardless of the condition of the tendon at the end effector. Therefore, the system does not fail even though there is no tendon control. The mechanism employs a feeder with a one-way clutch. The space efficiency of the spool allows this actuator to be smaller than a linear actuator. Details of the design concept are presented in Section III. Since the slack enabling mechanism operates by means of friction force, controllability, efficiency, and durability must be carefully considered. System modeling for control factors is provided in Section IV, and design optimizations to increase durability and efficiency are outlined in Section V. Finally, in Section VI we describe the development of a prototype slack enabling mechanism and demonstrate its performance by applying it to Exo-Glove, a soft wearable robotic hand.

## II. ADVANTAGES OF THE SLACK ENABLING MECHANISM IN SOFT ROBOTS

### A. Mechanical Prevention of Derailing of the Tendon from the Spool

A spool and motor combination is one of the most convenient and commonly used actuation methods for a tendon drive system. In this system, the tendon around the spool should always be under tension to prevent derailing. If the tendon derails, the system will fail. The amount of tension needed to prevent derailing is related to the bending stiffness of the tendon and the radius of the pulley. A higher bending stiffness and a smaller pulley radius will increase the required tension.

To maintain tension, the tendon is pre-tensioned via a tension control in many systems. However, tension control complicates a system that might not otherwise require tension control. In addition, stability is not guaranteed when the system is turned off. Furthermore, it is hard for the feedback controller to react to the external impact owing to the limited bandwidth of the feedback loop and it may lead to the failure of the system [15]. To overcome the limited bandwidth of the control, the target pre-tension must be higher than the minimum tension needed to prevent derailment. However, pre-tensioning can cause several issues which are explored in Section II-C.

### B. Actuation of Multiple Tendons with a Single Actuator

Some soft robots use multiple tendons for actuation. Multiple tendons enable antagonistic actuation and multi-plane movements of the soft body. The total number of actuators needed can be reduced if a single actuator can drive multiple tendons simultaneously. This can potentially increase a robot's compactness and efficiency.

However, because of the kinematic properties of soft robots, tendons will slacken if they are simply connected to a single actuator. The relationship between joint movement and tendon length is nonlinear and changeable because of deformation of the soft structure. Therefore, unless individual tendons are tensioned, multiple spools cannot be used with a single actuator because slackening will cause derailment.

A slack enabling mechanism makes it possible to actuate

multiple tendons with a single actuator by using multiple spools in an array. To use a spool array, the individual tendons should be tensioned using a mechanical structure. The slack enabling mechanism which will be described in Section III meets this requirement.

### C. Elimination of Safety and Efficiency Issues Related to Pre-tensioning

A slack enabling mechanism can increase efficiency by eliminating the need for pre-tension. Tendon pre-tension is closely related to the oppositional forces at play in antagonistic actuation. In an antagonistic actuation system, when one tendon is pulled to rotate a joint, the pre-tension of the opposite tendon resists the movement. This resistance decreases efficiency and can even cause a system malfunction. Furthermore, pre-tension induces a friction force along the tendon route that increases the level of resistance to movement. Friction-reducing components along the tendon path such as pulleys are difficult to implement in soft wearable robots, so the friction effect should be carefully considered. As the tendon slides on the surface of the tendon path, the friction models of the tendon-driven system follow the capstan equation, which explains the tension change along the tendon route [18]. According to the capstan equation, the tension applied to a joint, which acts to oppose the joint's movement, is exponential with the bending angle of the tendon, which means that the oppositional force becomes very large if the path of the tendon has many curves. Additionally, the oppositional force changes when the tendon path is changed, which makes it hard to control.

In the case for soft wearable robotics, a slack enabling mechanism can reduce risks of injury induced by pre-tension. Because a soft wearable robot is made of soft material and has no joints, tension on the tendon is directly applied to the wearer's skin and joints. Therefore, when a user wears the robot, pre-tensioning leads to continuous pressure on the skin and the joints, which can cause injuries such as pressure sores and arthritis. Moreover, to overcome the oppositional force induced by friction, the actuation tension needs to be high, which only increases the force applied to the body.

To handle the problems posed by pre-tension and the resulting oppositional forces, the tension of the antagonistic tendon must be minimized. This can be achieved by eliminating the tension applied by the antagonistic actuator. The slack enabling mechanism proposed in this paper can eliminate tension on the tendon by pushing the tendon from the actuator.

## III. DESIGN CONCEPT OF THE SLACK ENABLING MECHANISM

### A. A Slack Enabling Mechanism Employing a Single Spool

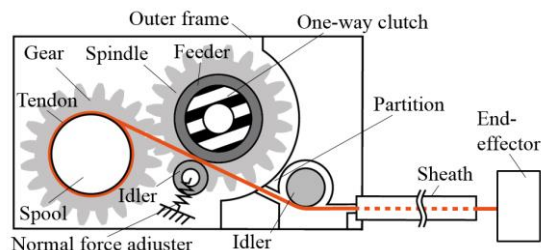


Fig. 1. Schematic of a slack enabling mechanism with one spool.

The schematic for a single-spool slack enabling mechanism is shown in Fig. 1. The basic idea is that a feeder and idler pair pulls the tendon from the spool by the friction force. The spool and shaft of the feeder are mechanically linked by the gear and pinion to allow the feeder and spool to be actuated by a single actuator.

The required action of the feeder, in order to always pull the tendon, depends on the movement of the spool. If the spool releases the tendon, the feeder, with the idler, should draw the tendon faster than the releasing speed of the spool. If the spool winds the tendon, the feeder and idler should exert a drag on the tendon.

To realize the required operation of the feeder, the rotation of the feeder shaft is selectively transmitted to the feeder by implementing a one-way clutch between the shaft and the feeder. Fig. 2 shows the movements of the main components and the force that the feeder applies to the tendon. As shown in Fig. 2 (a), when the spool unwinds the tendon, the feeder is forced to rotate, whereas the feeder does not rotate when the spool winds the tendon, as shown in Fig. 2 (b). As the spool winds the tendon, rolling resistance and friction force against the rotation of the feeder exert a drag on the tendon and apply force to it. Additionally, the radii of the spool and feeder, as well as the transmission between them, are designed to make the linear velocity at the surface of the feeder faster than the tendon unwinding speed of the spool.

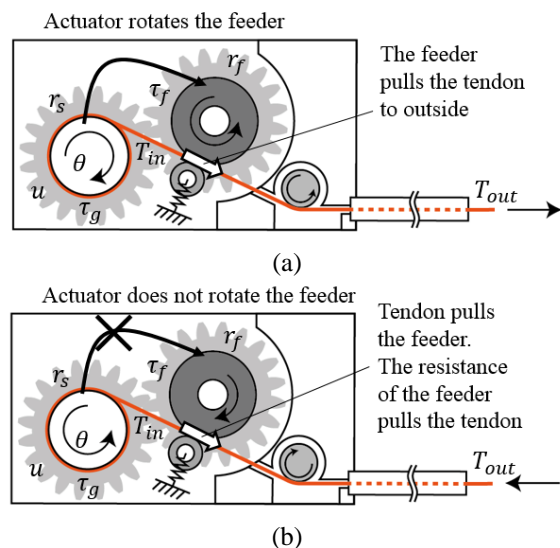


Fig. 2. Schematic diagram of behavior of the slack enabling mechanism while the spool (a) unwinds and (b) winds the tendon. Since the one-way clutch transmits power in one direction, the rotation of the actuator is not transmitted to the feeder when the tendon is wound. The white arrows indicate the force applied to the tendon from the feeder.

Because the system always tensions the tendon from the spool, the system is restored to a stable state even after the tendon around the spool is loosened.

### B. A Slack Enabling Mechanism Employing Multiple Spools

The slack enabling mechanism can be expanded to an array with multiple spools, which allows a single actuator to drive multiple tendons. Fig. 3 shows the slack enabling mechanism used for a pair of spools. Two spools and two feeders are

stacked on their axes. As in the single-spool case, the axes of the spools and feeders are mechanically linked by a gear pair.

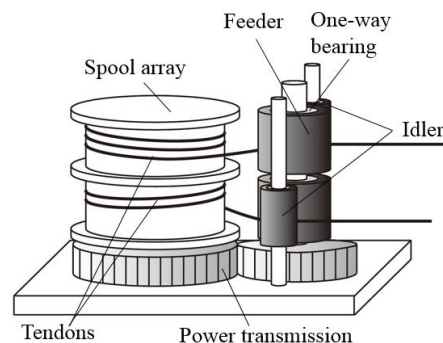


Fig. 3. Schematic of a slack enabling mechanism with multiple spools.

One of the most important considerations for driving tendons with a multi-spool array is the excursion ratio and driving direction of the tendons. Generally, the required excursion for multiple tendons varies depending on the application. A pair of tendons that are connected in opposite directions allows a single actuator to be used as an antagonistic actuator.

The ratio of the excursion of each tendon is adjusted by changing the ratio of the radius of each spool. Because the linear velocity of the feeder should be greater than the linear velocity of the spool, the radius of each feeder is designed with respect to the spool radius. To match the linear velocity of the feeders, the idlers that share the axis should rotate at different speeds. Therefore, each idler should have an independent, freely rotating bearing.

A tendon can be actuated in the opposite direction from the other tendons by installing it in the opposite direction on the spool. To avoid having to increase the number of feeder axes and feeder-spool transmission components, all the feeders should be installed on a single shaft. The feeders for the reversely installed tendons are installed by changing the direction of the one-way clutch, and the tendons contact the feeder on opposite sides.

Because all the requirements can be satisfied regardless of the number of tendons, in theory the slack enabling mechanism is expandable to an unlimited number of spools.

### C. Comparison of the Slack Enabling Mechanism with a Ball Screw

The objective of the slack enabling mechanism may also be achieved by using a linear actuator. The linear actuator inherently allows tendon slack since the tendon route is closed and the tendon cannot be derailed from the intended path. However, the proposed slack enabling mechanism has size and form factor advantages compared with the linear actuator. Since the mechanism for a linear actuator must be longer than the required excursion length of the tendon, the size of the linear actuation mechanism enlarges when the application requires a longer stroke.

Various mechanisms construct linear actuators, such as a ball screw, a pneumatic or hydraulic cylinder, or an air muscle. As the mechanism driven by the electrical motor, the size of the ball screw and the proposed slack enabling mechanism should

be compared.

The dimensions of the ball screw and the slack-enabling actuator are compared in Fig. 4. The size of the mechanisms is evaluated according to the volume of the outer circumscribed cube by taking account of the outer casing of the final product. The size of the ball screw and the slack enabling actuator is expressed in (1) and (2), respectively:

$$V_{BS} = 4R_{nut}^2(L + L_{nut}) \quad (1)$$

$$V_{SE} = 4R_g(R_g + R_p)(H_s + H_g) \quad (2)$$

$$H_s = \frac{Ld}{2\pi R_s} \quad (2-1)$$

where  $L$  is the required excursion length of the tendon and  $d$  represents the diameter of the tendon. The other parameters are shown in Fig. 4.

Based on the volume of the components, the weight of the slack enabling structure and ball screw are presented as

$$W_{BS} = \rho_s \pi (R_{nut}^2 L_{nut} + R_{shaft}^2 L) \quad (1^*)$$

$$W_{SE} = \rho_s \pi (H_g (R_g^2 + R_p^2) + H_s R_s^2) + \rho_r \pi H_s R_f^2 \quad (2^*)$$

where  $\rho_s$  is the density of steel and  $\rho_r$  is the density of rubber which is used for feeder.

### 1) Size of the slack enabling mechanism

The major constraint on the size of the slack enabling actuator derives from the limitation of reducing the radius of the spool. As tendon diameter increases and the tendon's yield strength decreases, the radius of the spool must increase to prevent plastic deformation of the tendon, which causes tendon failure.

The height of the spool is related to the required excursion length of the tendon. The ability of the spool to accommodate the maximum winding length of the tendon is determined by the product of the circumference and the height of the spool.

Because the force required on the feeder and the idler is small (as will be shown in Section V, "Design Considerations"), the force capability of the mechanism to transmit the rotation from the spool to the feeder is not a consideration. Therefore, the height of the gear pairs is only determined by the height of the affordable one-way clutch. The gear connected to the spool should have a larger diameter than the spool because the velocity of the surface of the feeder must be faster than the unwinding velocity of the spool. Therefore,  $R_g$  presented in equation (2) should be bigger than  $R_p$ . The diameter of the gear connected to the spool is determined by the minimum diameter of the affordable gear. The diameter of the feeder is selected to be the same as that of the connected pinion.

### 2) Size of the ball screw mechanism

The main factor determining the size of the ball screw is the required excursion length of the tendon. The ball screw must be longer than the required stroke of the tendon.

The cross-sectional area of the ball screw system is determined by the diameter of the nut. The nut is selected based on the diameter of the screw, which determines the screw's ability to prevent buckling of the screw induced by the tension

of the tendon [19], which can be expressed as

$$P = 0.5 \frac{\eta \pi^2 E I}{L_{screw}^2} \quad (3)$$

where  $P$  is the permissible load,  $\eta$  is the factor relating to the mounting method,  $E$  is Young's modulus of the material of the screw,  $I$  is the area moment of the inertia of the screw, and  $L_{screw}$  is the length of the screw. Maximum  $\eta$  is 4 when both ends of the screw are axially fixed by bearings.

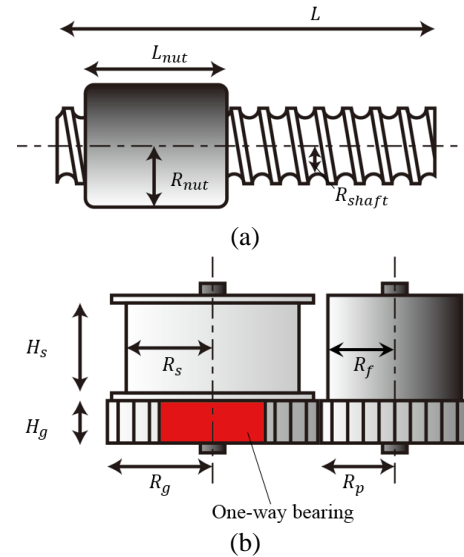


Fig. 4. Dimensions of (a) a linear actuator and (b) a slack enabling actuator. The red area in (b) is the one-way clutch installed at the center of the gear.

### 3) Size of both mechanisms with affordable component and slack enabling mechanism prototype

The size of the slack enabling mechanism and the ball screw may also be compared in terms of the requirements of a specific application. For example, the maximum tension and excursion length of the Exo-Glove tendon is 80 N and 200 mm, respectively. The design parameters of the slack enabling mechanism and the ball screw and the components satisfying the requirements are shown in Table 1. In order to achieve adaptive grasping, the tendon path of Exo-Glove is similar with the path of the tendon connected to the moving pulley. Due to the unique tendon path and deformation of the structure, Exo-Glove requires more than double excursion length as long as typical exoskeleton requires.

Fig. 5 presents the relationship between the size and weight of the slack enabling mechanism and the ball screw and the required excursion length of the tendon. As shown in the graph, the slack enabling mechanism requires a smaller volume except when the excursion distance of the tendon is very limited.

Fig. 6 depicts a prototype of the slack enabling mechanism with a single spool. The components were made with a three-dimensional printer (Connex 260, Stratasys Ltd.), and the material was VeroWhite (Stratasys Ltd.). The final size of the prototype was enlarged by the outer frame that holds the core components, but even so the entire size of the prototype is smaller than the core component of the ball screw.

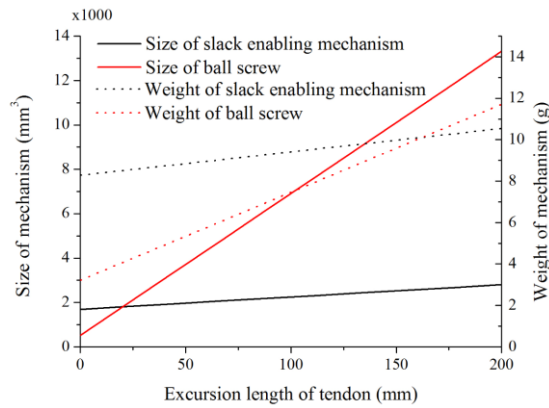


Fig. 5. Size and weight of the slack enabling mechanism and the ball screw with respect to the required excursion length of the tendon.

TABLE 1  
DESIGN PARAMETERS FOR BUILDING A SLACK ENABLING ACTUATOR AND A BALL SCREW FOR EXO-GLOVE

Requirements for Exo-Glove		
Required spec	Tension	80 N
	Excursion length	200 mm
Parameters of selected components of the slack enabling mechanism		
Tendon	Maximum tension	80 N
	Diameter	0.53 mm
	Permissible curvature	$>1/5 \text{ mm}^{-1}$
One-way clutch	Outer diameter	7.2 mm
	Height	5.4 mm
Spool	Spool diameter	9 mm
	Flange diameter	11 mm
	Flange thickness	1 mm
Gear and pinion	Gear height	5.4 mm
	Gear diameter	12 mm
	Pinion diameter	10 mm
Feeder	Feeder diameter	8 mm
Parameters for selected components of the ball screw		
Required spec	Minimum screw diameter	2 mm
	Screw diameter	2.6 mm
Chosen ball screw	Nut diameter	8 mm
	Nut length	8 mm

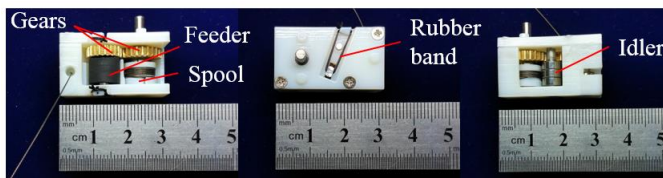


Fig. 6. Front, top, and back side of the prototype. Device dimensions are  $32 \times 18.5 \times 18$  mm. Rubber band is used to push the idler toward the feeder.

#### IV. MODELING

This section describes the model of the slack enabling actuator, showing how the friction forces inside the actuator interact. This model is suitable for designing a controller for the actuator (discussed in Section VI-B).

#### A. Single Spool Actuator

Fig. 2 illustrates the interaction of forces inside the actuator as the actuator unwinds and winds the tendon. The inertia of the rotating part and the tendon is not considered because the friction forces inside the actuator are much more dominant than the inertial forces. The key point of this model is that the friction force is always exerted on the wire so that the tension of the wire inside the actuator is positive when using a one-way clutch. Table 2 describes the parameters used in this model.

TABLE 2  
MODELING SYMBOLS

Symbol	Quantity	Units
$u$	Torque input of the motor	$Nm$
$w$	Angular velocity of the motor	$rad/s$
$\theta$	Angle of the motor spool	$rad$
$\tau_g$	Friction of the motor gearbox	$Nm$
$\tau_f$	Torque applied to the motor from the feeder through the one-way clutch	$Nm$
$T_{in}$	Tension of the wire between the spool and the feeder	$N$
$T_{out}$	Tension of the wire on the output port	$N$
$F_f$	Friction force between the feeder and the wire	$N$
$R_s$	Radius of the motor spool	$mm$
$R_f$	Radius of the feeder	$mm$
$F_N$	Normal force of the idler	$N$
$\mu$	Friction coefficient between feeder and wire	

Motor side:

$$u = \pm \tau_g + R_s T_{in} - \tau_f \quad (4)$$

$$\begin{cases} w < 0, & \tau_f = R_f F_f \\ w > 0, & \tau_f = 0 \end{cases} \quad (5)$$

Wire side:

$$T_{in} = T_{out} + F_f \quad (6)$$

Here,  $\tau_f$  describes the torque transmitted from the feeder to the motor shaft through spur gears and the one-way clutch. It should never be a negative value because torque is transmitted in one direction via a one-way clutch. Therefore,  $\tau_f$  is positive and zero, respectively, when the actuator unwinds and winds the wire. The actuation principle described above can be written as shown in (5). Here, the friction force between the wire and the feeder is assumed to be proportional to the normal force of the idler. Equation (6) indicates that the inner tension of the actuator is always positive since the output tension of the actuator never becomes negative unless the wire is compressed. Combining (4)–(6) results in the following:

$$u = \begin{cases} (w < 0) & R_s T_{out} + R_s F_f + \tau_g - R_f F_f \\ (w > 0) & R_s T_{out} + R_s F_f - \tau_g \end{cases} \quad (7)$$

## B. Dual Spool Actuator

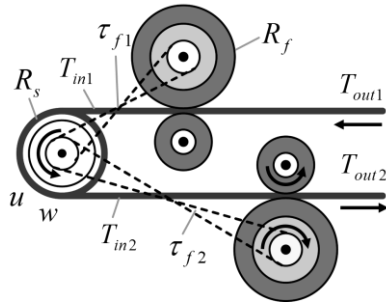


Fig. 7. Schematic of a dual spool slack enabling actuator.

The model for a multiple spool actuator follows the same modeling rule as a single spool actuator. This section describes the model for dual spools operating opposite to each other, as shown in Fig. 7. Applying the principle in (4)–(6) results in the following:

Motor side:

$$u = \pm\tau_g + R_s T_{in1} - R_s T_{in2} - \tau_{f1} + \tau_{f2} \quad (8)$$

In the case of winding wire 1 and unwinding wire 2, the torque transmitted through the one-way clutch is as follows:

$$\begin{aligned} \tau_{f1} &= 0 \\ \tau_{f2} &= R_f F_{f1} \end{aligned} \quad (9)$$

In the other case of unwinding wire 1 and winding wire 2, the torque transmitted through feeder 2 becomes zero and the torque transmitted through feeder 1 is a positive value.

Tendon 1 side:

$$T_{in} = T_{out1} + F_{f1} \quad (10)$$

Tendon 2 side:

$$T_{in2} = T_{out2} + F_{f2} \quad (11)$$

Combining (9)–(11) results in

$$u = \begin{cases} (w > 0) & R_s(T_{out1} - T_{out2}) + R_s(F_{f1} - F_{f2}) + \tau_g + R_f F_{f1} \\ (w < 0) & R_s(T_{out1} - T_{out2}) + R_s(F_{f1} - F_{f2}) - \tau_g - R_f F_{f2} \end{cases} \quad (12)$$

If the actuator is designed to have the same friction forces as the feeders (same material, shape, and normal force),  $F_{f1} = F_{f2}$ , (12) is reduced to

$$u = R_s(T_{out1} - T_{out2}) + (\tau_g + R_f F_f) \cdot \text{sgn}(w) \quad (13)$$

Equation (13) indicates that the actuator experiences the same amount of friction force when moving in either direction. The slack-enabling actuator does not apply tension on both sides of the wire at the same time, making at least one wire slack. Therefore,  $T_{out1}$  and  $T_{out2}$  in (13) can be reduced to  $T$  with a different sign that depends on the direction of the actuation:

$$u = \pm R_s T + (\tau_g + r_f F_f) \cdot \text{sgn}(w) \quad (14)$$

## V. DESIGN CONSIDERATIONS

### A. Design Parameters Affecting Performance

The main criteria for actuator performance are durability of components, stability of operation, and efficiency. Durability, stability, and efficiency are affected by the normal force between the feeder and the tendon. A higher normal force increases stability but decreases durability and efficiency.

Because the friction force and rolling resistance increase as the normal force increases [20], a smaller normal force has an advantage in terms of efficiency. According to the Archard wear equation [21], wear on the feeder and the tendon, which slip against each other, is proportional to the sliding distance and the normal force between the feeder and the tendon. Therefore, to increase efficiency and durability, a small normal force between the tendon and the feeder is preferred. However, if the normal force is too small, the friction force available to tense the tendon around the spool also decreases, which can cause instability. Therefore, the normal force should be optimized at the minimum value that can maintain the tendon around the spool tightly.

The optimal normal force between the feeder and the idler will be explored in next section.

### B. Design Parameters Related to Tightening the Tendon around the Spool

#### 1) Parameters in play when the tendon is wrapped around the spool

Fig. 8 shows the parameters that affect the path of the tendon. The three circles in the figure indicate spool, feeder and idler. The biggest circle indicates the spool, and the thick line is the tendon. The tendon is wrapped around the spool, and it departs from the spool at point indicated by  $\theta_0$ , which is termed the departing point. The red-colored arc indicates the small part of the tendon that is in contact with the spool. The force and moment applied to the red arc are represented in the figure.

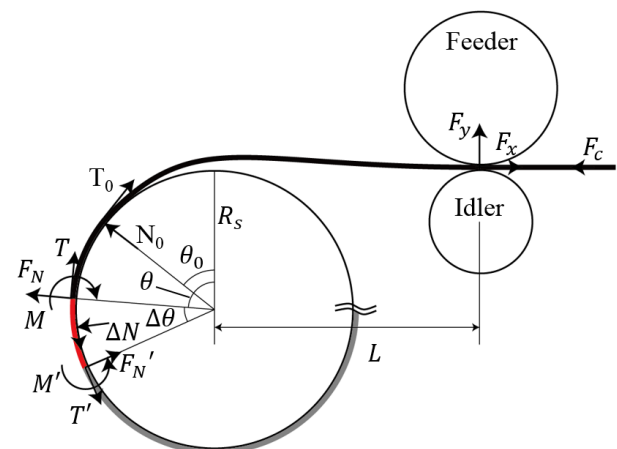


Fig. 8. Force being applied to the tendon around the spool.

According to the beam-bending model, the moment  $M$  is determined by

$$M = \frac{1}{R_s} EI \quad (15)$$

where  $R$  is the radius of the spool and  $EI$  is the bending stiffness of the tendon. The thickness of the tendon is not considered in calculating the curvature because it is much smaller than the radius of the spool.

The moment change along the tendon can be determined by the moment equilibrium on the arc as shown in Fig. 8, which is

$$\Delta M = -F_N R_s \sin \Delta\theta + R_s T (1 - \cos \Delta\theta) - \Delta N R_s \sin \frac{\Delta\theta}{2} + \mu \Delta N R_s \left(1 - \cos \frac{\Delta\theta}{2}\right) \quad (16)$$

$$dM = F_N R_s d\theta \quad (16-1)$$

where  $F_N$  is the internal force in the transverse direction,  $\Delta\theta$  is the central angle of the arc,  $\Delta N$  is the distributed force applied to the tendon from the spool, and  $T$  is the tension of the tendon. When the infinitesimally small fraction is considered, the equation can be rewritten as (16-1), which shows that the internal force in the transverse direction of the tendon only affects the moment change along the arc. Positive  $F_N$  increases the curvature of the tendon, whereas negative  $F_N$  decreases the curvature. Therefore, in order to maintain the moment that keeps the tendon well wound around the spool,  $F_N$  should be zero. At the departing point, the normal force  $N_0$  should cancel out the force applied to the tendon in the normal direction. Along the tendon, variation of  $F_N$  is obtained by the force equilibrium condition, which can be expressed as

$$F'_N = F_N \cos \Delta\theta - T \sin \Delta\theta + \Delta N \cos \frac{\Delta\theta}{2} + \mu \Delta N \sin \frac{\Delta\theta}{2} \quad (17)$$

$$dF_N = -T d\theta + dN \quad (17-1)$$

Because  $F_N$  should be zero constantly, the deviation of  $F_N$  should be zero. Since the reaction force from the spool must be positive, when the tension of the tendon is below zero the reaction force cannot cancel out the normal force generated by the tension term. Consequently, to tighten the tendon around the spool, the tension of the tendon should be positive. Because the friction force generated by the reaction force from the spool is applied to the tendon where it departs from the spool, the tension at the departing point should satisfy (18):

$$T_0 > \mu N_0 \quad (18)$$

The required force that should be applied to the tendon from the feeder to meet the condition presented in this section is explored in following section.

## 2) Parameters in play at the tendon's point of departure from the spool

The force and moment applied to the tendon at the departing point are determined by the force applied to the tendon from the

feeder and the idler as well by as the geometry of the spool and the feeder. According to the condition presented in the previous section, the force applied from the feeder and the idler should generate positive tension at the departing point. The critical condition to satisfy the requirement of zero tension at the departing point is affected by the path of the tendon. By considering the friction force between the tendon and the spool at the departing point, the force from the feeder should satisfy this force equilibrium equation:

$$R(\theta_0) \begin{bmatrix} F_x \\ F_y \end{bmatrix} - \begin{bmatrix} \mu N_0 \\ N_0 \end{bmatrix} = \begin{bmatrix} 0 \\ 0 \end{bmatrix} \quad (19)$$

where  $F_x$  and  $F_y$  represent the force exerted by the feeder and the idler and  $\mu N_0$  and  $N_0$  represent the friction force and normal force at the departing point.  $\theta_0$  represents the angle indicating the departing point. Since  $F_x$ ,  $F_y$ , and  $\theta_0$  are related each other, the minimum  $F_x$  and  $F_y$  is explored by considering the tendon path. The path of the tendon is determined by the curvature along the tendon, which is expressed as

$$\kappa = -\frac{y''}{(1+y'^2)^{3/2}} \quad (20)$$

where the derivative is with respect to the  $x$  position of tendon. According to equation (15), the path of the tendon is rewritten as

$$y'' + \frac{M}{EI} (1 + y'^2)^{\frac{3}{2}} = 0 \quad (21)$$

where  $M$  represents the moment along the tendon, which can be expressed as

$$M = M_a + F_x(y - y_a) - F_y(x - x_a) \quad (22)$$

where  $M_a$  represents the moment, and  $F_x$  and  $F_y$  represent the forces at the departing part. By employing dimensionless parameters, equations (21) and (22) can be rewritten as (21-1) and (22-1):

$$y^{*''} + \frac{R_s M}{EI} (1 + y^{*'}{}^2)^{\frac{3}{2}} = 0 \quad (21-1)$$

$$\frac{R_s M}{EI} = 1 + \frac{R_s^2 F_x}{EI} (y^* - y_a^*) - \frac{R_s^2 F_y}{EI} (x^* - x_a^*) \quad (22-1)$$

where  $x^*$ ,  $x_a^*$ ,  $y^*$ , and  $y_a^*$  mean  $x/R_s$ ,  $x_a/R_s$ ,  $y/R_s$ , and  $y_a/R_s$ , respectively. By the geometrical condition at the departing point of the tendon from the spool and the contact point of the tendon with the feeder, the boundary conditions shown in (23)–(27) are obtained:

$$x_a^* = x_0^* - \sin \theta_0 \quad (23)$$

$$y_a^* = y_0^* + \cos \theta_0 \quad (24)$$

$$y_a^{*'} = \tan \theta_0 \quad (25)$$

$$y_b^* = 0 \quad (26)$$

$$y_b^{*'} = 0 \quad (27)$$

where  $x_0^*$  and  $y_0^*$  indicate the position of the spool divided by the radius of the spool. To avoid bending the tendon while it passes the feeder,  $y_0^*$  is fixed as -1. Using the boundary conditions and according to equations (21-1) and (22-1), the minimum force exerted by the feeder and the idler with respect to  $x_0^*$  and the friction coefficient between the spool and the tendon can be shown (Fig. 10 [a]). As the graphs show, the required tension is not changed much by the position of the spool and increases as the friction coefficient increases.

To verify the simulation result, we conducted an experiment to measure the required minimum pulling force to wrap the tendon around the spool. The experimental setup is shown in Fig. 9. At first, the tendon was installed to a pin vice that was installed at the load cell. After that, the tendon was loosely wrapped around the spool at the center. The distance from the end of the pin vice to the spool was set as three times the radius of the spool.

The opposite end of the tendon was fixed to an appropriate position at the ground so that the tendon around the spool was not tightened. After that, the load cell was moved to pull the tendon. The force at the moment when the tendon around the spool was tightened was measured as the tension required to wrap the tendon around the spool.

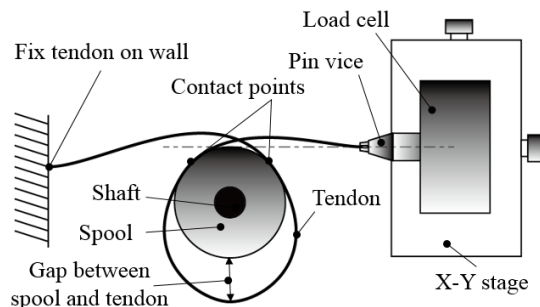


Fig. 9. Experimental setup to measure the minimum force to wrap the tendon around the spool.

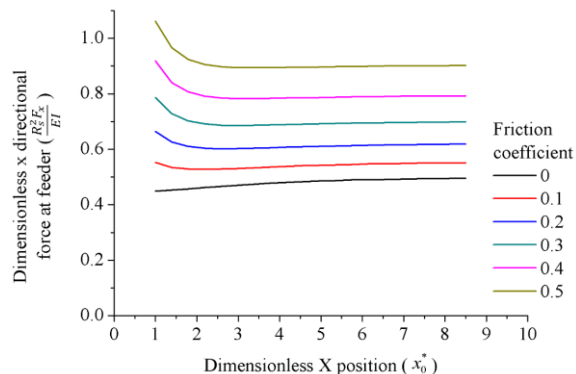
TABLE 3  
MECHANICAL PROPERTIES OF TENDONS USED IN THE MINIMUM REQUIRED PULLING FORCE EXPERIMENT.

	Material	Diameter	Bending stiffness
Tendon 1	Stainless steel (7 stranded)	0.67 mm	146 Nmm <sup>2</sup>
Tendon 2	Stainless steel (7 stranded)	0.58 mm	84 Nmm <sup>2</sup>
Tendon 3	Nylon-coated titanium (7 stranded)	0.53 mm	9 Nmm <sup>2</sup>

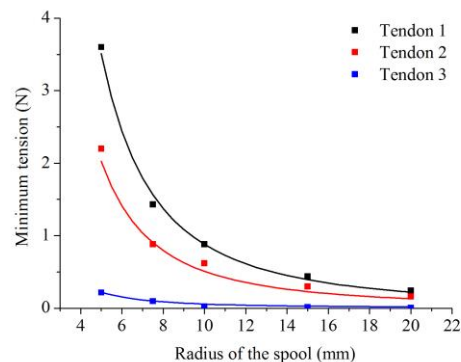
To verify how the required tension varied with respect to tendon properties and the diameter of the spool, three different tendons and five spools of different diameters (5, 7.5, 10, 15, and 20 mm) were used in the experiment. The characteristics of the tendons are shown in Table 3.

The experimental data and the simulation data are compared in Fig. 10. The friction coefficient used in the simulation is 0.19 as measured. As shown in the figure, the required minimum force to tighten the tendon around the spool follows the

simulation result well.



(a)



(b)

Fig. 10. Required force at the feeder to wrap the tendon around the spool. (a) Simulation result for the variation of the dimensionless x position and the dimensionless minimum tension with respect to the change of friction coefficient between the tendon and the spool. (b) Comparison of the simulation and the experimental data for three different tendons with respect to spool radius.

### 3) Parameters related to the compression force exerted on the tendon

Compression force can be applied to the tendon if it is stuck in the sheath or by the end-effector during tendon release. Compression force decreases the tension applied to the tendon between the spool and the feeder. Consequently, tendon tension decreases below the critical condition. To limit the compression force, the tendon is exposed between the feeder and the entrance of the sheath. When the compression force exceeds a certain level, the exposed tendon buckles, and the compression force is not increased even if the tendon is stuck outside. While the tendon buckles, the maximum compression force is affected by the bending angle of the tendon between the feeder and the sheath as well as by the exposed length of the tendon. The compression force with respect to the path of the tendon can be derived by modifying the beam-bending model used in the previous section, which is

$$y^{+''} + \frac{dM}{EI} (1 + y^{+'2})^{\frac{3}{2}} = 0 \quad (21-2)$$

where  $d$  represents the distance from the contact point of the tendon and the feeder to the entrance of the sheath, and  $y^{+'}$

represents  $y/d$ . The boundary conditions for compression force analysis are as follows:

$$x_a^+ = 0 \quad (28)$$

$$x_b^+ = d \quad (29)$$

$$y_a^{+'} = -\tan\frac{q}{2} \quad (30)$$

$$y_b^{+'} = \tan\frac{q}{2} \quad (31)$$

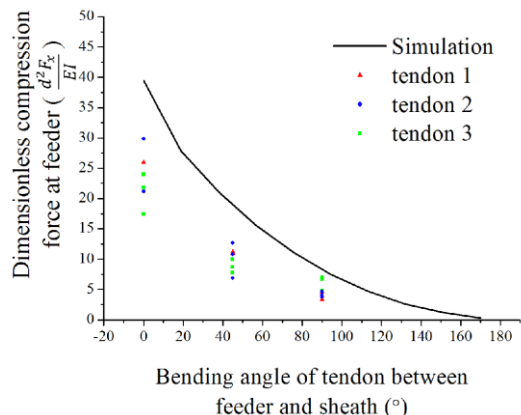


Fig. 11. Maximum compression force with respect to tendon angle change and distance.

The trend of the maximum compression force is presented in Fig. 11. The black line represents the simulation result, and the dots are the experimental data for the tendons shown in Table 3. The experimental setup shown in Fig. 12 was used to measure the maximum compression force. In Fig. 12, the tube stands for the sheath of the real prototype, and the compression force at the feeder is measured by the load cell. As the experimenter pushed the tendon into the tubes, the compression force applied to the tendon was measured. The gray lines represent the change of the tendon path as the tendon is pushed. The compression force increases at first but decreases after the tendon buckles. The experiment was conducted by changing the distance from the pin vice to the tube in 10 mm, 20 mm, and 30 mm increments.

As shown in Fig. 11, the simulation result is always larger than the experimental data. First, the bending angle of the experiment is larger than we expected because of the tolerance between the tube and the tendon. Second, the curvature of the tendon around the tube and the pin vice is too large, which decreases the bending stiffness of the tendon [22]. Since the both factors decrease the maximum compression force, the simulation result is acceptable for use in the design.

#### 4) Parameters related to the required normal force between feeder and tendon

The source of the force that maintains tension and produces the compression force is friction between the tendon and the feeder. The friction force is proportional to the normal force between the tendon and the feeder.

To adjust the normal force between the feeder and the tendon, the shaft of the idler is designed to be pushed toward the feeder. The force pushing the shaft must generate appropriate friction force at the feeder. The friction force must be greater than the

summation of the minimum tension and the maximum compression force. Owing to unexpected perturbation and dynamic forces, the tendon can be slackened during operation when the friction force is on the borderline. To overcome this limitation, a little bit higher friction force than was predicted from the analysis should be applied for practical use.

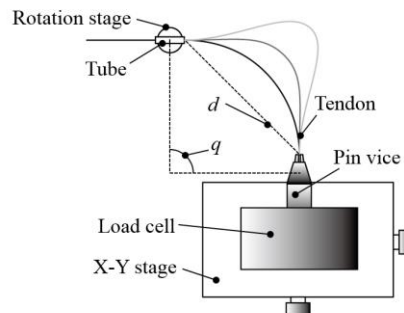


Fig. 12. Experimental setup to measure the maximum compression force that can be applied to the tendon.

Tendon 3 in Table 3 is the one used in Exo-Glove. The diameter of the spool is 9 mm. According to the model, the required minimum tension is 0.25 N, and the maximum compression force that can be applied to the tendon is 0.5 N. By considering the friction coefficient between the feeder and the tendon (which is 0.5), 1.5 N is required as the normal force between the feeder and the tendon. For stable operation even with unexpected perturbation, 3 N was selected as the pushing force to be applied to the shaft of the idler.

## VI. APPLICATION AND PERFORMANCE

### A. Application: Exo-Glove

The performance of the slack enabling mechanism was demonstrated by applying a prototype actuator with dual spools and a single actuator to Exo-Glove (Fig. 13) [13]. Exo-Glove is a soft wearable robotic hand constructed of fabric and driven by multiple tendons. The tendons connect to the front and the back of the digits and the actuator through a Bowden cable sheath. By actuating the tendons, Exo-Glove helps flex and extend the thumb, index, and middle fingers, giving people with hand paralysis a functional grip. To achieve an adaptive grasp, flexion of the index and middle fingers is accomplished by a single tendon that passes a specially designed path over the front of the fingers.

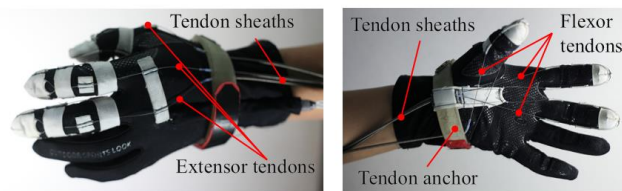


Fig. 13. Exo-Glove. Three extensor tendons are connected to the index finger, middle fingers, and thumb to extend each digit. Two flexor tendons are used, one for the thumb and the other for the index and middle fingers. The flexor for the index and middle fingers forms a differential mechanism so that the index and middle fingers can flex adaptively to the shape of the grasped object.

Fig. 14 shows the kinematic nonlinearity of Exo-Glove. The graph shows the pulled length of the flexor and extensor

tendons that Exo-Glove required to grasp various sized cylindrical objects. The pulled length was measured compared with the fully extended position. The index finger was more extended when grasping a larger object. Since the moment arm of the flexor tendon to the finger joint changed with respect to the posture of the finger, the pulled length shows nonlinearity. Moreover, owing to the compliance of the structure, the pulled length of the flexor tendon increases when the applied force increases.

In spite of this kinematic nonlinearity, Exo-Glove was driven without actuator failure because the slack enabling actuator can operate when the tendons are slack.

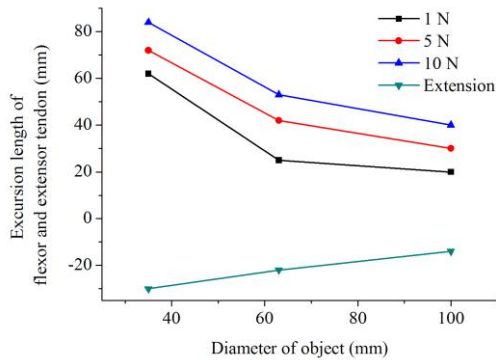


Fig. 14. Kinematics of Exo-Glove. The pulled or released length of the flexor and extensor tendons is shown with respect to the diameter of grasped cylindrical objects. The references of the tendon positions are set as the positions when the fingers are fully extended. The pulled length of the flexors varies as the tension applied to the tendon changes.

Table 4 shows the results of another experiment on the effect of tension at the antagonist. This experiment compared extension motions of the index finger actuated with and without pre-tension on the flexor tendon. When the flexor was pre-tensed, the flexor tendon of Exo-Glove was tensed by applying balance weights of 20 g and 100 g. When the flexor was not pre-tensed, the prototype slack enabling actuator was used for actuation. The angle of the metacarpal (MCP) joint, proximal interphalangeal (PIP) joint, and distal interphalangeal (DIP) joint was measured as the extensor tendon pulled the finger with 50 N. The angle change from the fully flexed position was compared with the fully extended posture. As shown in Table 4, the application of even very small amounts of tension to the flexor tendon severely restricted the extension motion.

TABLE 4

EXTENSION COVERAGE OF THE INDEX FINGER WITH RESPECT TO DIFFERENT PRE-TENSION CONDITIONS ON THE FLEXOR TENDON

Pretension	MCP	PIP	DIP
No pre-tension	>100 %	>100 %	>100 %
0.2 N	37 %	88 %	80 %
1 N	14 %	54 %	35 %

### B. Control Strategy

The admittance controller, which is a position-based impedance controller [23], [24], was adopted to provide compliant interaction between the actuator, transmission, human body, and environment. The admittance controller

calculates the reference position,  $x_{ref}$ , based on the desired impedance, equilibrium position,  $x_{eq}$ , and external force,  $F_{ext}$ , which is represented as

$$m\ddot{x}_{ref} + c\dot{x}_{ref} + k(x_{eq} - x_{ref}) = F_{ext} \quad (32)$$

where  $m$ ,  $c$ , and  $k$  represent the impedance of the inertia, damping coefficient, and spring coefficient, respectively, and  $F_{ext}$  is the external force exerted on the wire. This control scheme is advantageous for a soft wearable robot with a soft tendon routing system because it provides robust performance. The reference trajectory of the position controller can easily be tuned with the impedance parameter. Additionally, the interaction force and reference position are regulated to the proper levels, although the position command exceeds the desired target position. The PD (proportional-derivative) controller was adopted to control the position of the wire to  $x_{ref}$ .  $F_{ext}$  can be measured with the tension sensor placed on the actuator side. The tension estimator was used to estimate  $F_{ext}$  with the current of the DC motor, using the actuator model from Section IV to decrease the size of the actuator.

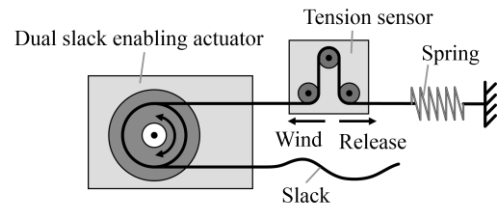


Fig. 15. Experimental setup to identify the lumped parameter of the model.

Fig. 15 shows an experiment that was conducted to decide the lumped parameter of the derived model. The normal forces of the idlers were set to the same value on both sides using the set screws and implemented springs on idlers with three different values. One output wire was connected to the linear spring to provide external force to the system when the actuator was winding and unwinding. The motor current and wire tension were measured using the signal from the motor driver and the tension sensor, respectively. Three periods of sinusoidal position trajectory were provided to the actuator, with the PD position controller at 0.5 Hz to negate the dynamic of the PD controller.

Fig. 16 shows the current of the motor with different normal forces and the tension exerted on the wire during winding and release. The motor current increases and decreases as the external tension increases and decreases. There is an offset for the current that is proportional to the normal force of the idler, which coincides with the derived friction model. Fig. 17 clearly shows the relationship between motor current and wire tension, which is a rearrangement of the data in Fig. 16. Clearly there are two stages depending on the direction of actuation of the wire. The offset increases with increasing normal force of the idler. The higher normal force guarantees more stable operation of the actuator by increasing the inner tension of the wire. But it consumes much power, decreasing the energy efficiency and maximum force capacity. The model parameters were fitted using the experimental data in Fig. 18. However, there is a

discrepancy between the slopes of the winding and the releasing states. This difference may have originated from the unmodeled friction between the wire and the output porthole of the actuator. In this case, the inlet and outlet tension of the wire is governed by the capstan formula [25], which describes the different slopes seen when winding and releasing the wire. Then we were able to estimate the external tension using the fitted model and the current of the motor, and fitted model was applied to the sensorless admittance controller.

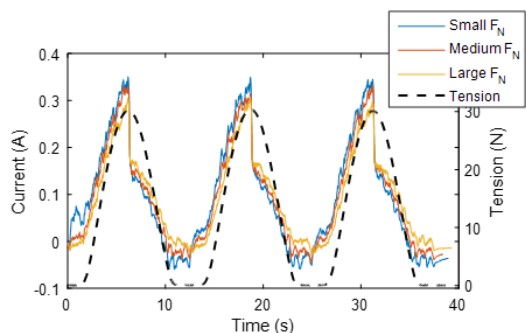


Fig. 16. Measured force and current of the DC motor while winding and releasing the wire connected to the linear spring with different normal forces  $F_N$

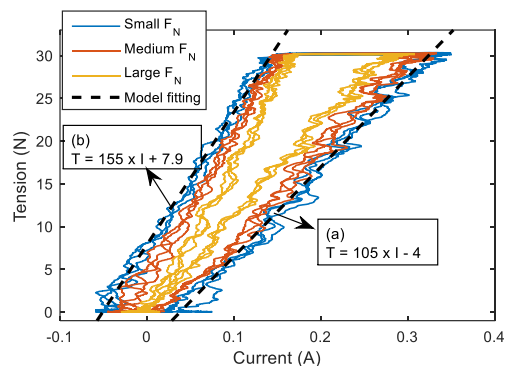


Fig. 17. Relationship between motor current and wire tension while (a) winding and (b) releasing the wire.

Fig. 18 shows the experimental setup to evaluate the performance of the actuator and the controller. The equilibrium position of the controller was fixed, and the external force was applied to the wire.

Fig. 19 shows the result of sensorless admittance control of the tendon actuator. The result indicates that the controller performs compliant interaction with the environment. In addition, the estimated force appropriately follows the measured force. However, the error increases near zero tension of the wire, which we considered to be originating from a fitting error of the model parameters on equation (14) and Fig. 17. The normal force exerted on the feeder of the current prototype is not stable. Also, although the reference position of the admittance controller was set to zero, results show that the position of the wire goes below zero, which we considered to be an error originating from the dead-zone of static friction.

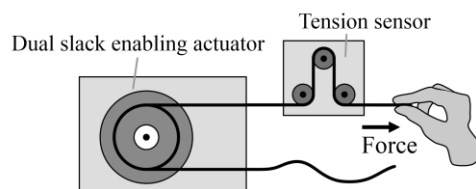


Fig. 18. Experiment to evaluate actuator performance.

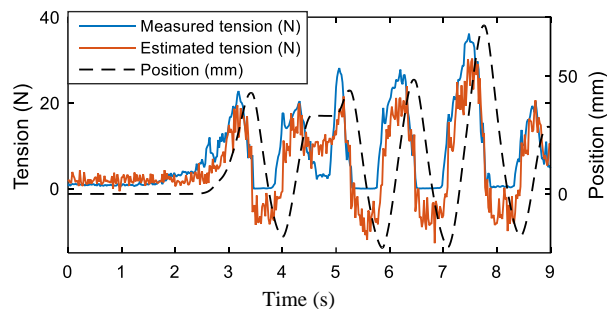


Fig. 19. Results of sensorless admittance control.

## VII. CONCLUSIONS AND FUTURE WORK

In soft robots, pre-tension of a tendon creates problems related to friction, nonlinear kinematics, and the application of force to the body of the robot. To deal with these issues, we have presented a novel tendon drive mechanism that allows slack during operation. This actuator eliminates the need for pre-tension.

Because the slack enabling actuator employs a spool, it is much smaller than a linear actuator. The slack enabling actuator is easily expanded to multiple spools with different diameters and actuating directions. Using multiple spools allows multiple tendons to be actuated in different ratios, and even antagonistic actuation is achievable with a single actuator.

Zero tension at the releasing tendon dramatically decreases the force applied to the soft robot structure driven by antagonistic tendon pairs, and this can prevent the structure from being squeezed with excessive force. In addition, control become easier because it is unnecessary to consider the tension and friction force at the antagonist. Because the tendon cannot be derailed from the spool without control, multiple tendons actuated by a single actuator can be used for robots that have nonlinear kinematics. Thanks to its small size, the slack enabling actuator enables a small-size system, even when the required excursion length of the tendon is quite long. For all these reasons, we believe that this actuator can be a fine option for soft wearable robots.

The slack enabling actuator has some limitations. First, the robot is easily perturbed toward the opposite direction of the slack tendon. Therefore, the slack enabling actuator is not suitable for the application which requires maintaining position in all directions. Second, with tendon slack, the system has dead zone; it is not adequate for the application which has reciprocating motion or requires fast response. In addition, the tendon of the slack enabling actuator suffers from being more bent compared with the tendon of a linear actuator, and friction force is applied to the tendon. Therefore, the tendon of the slack enabling actuator wears out faster than the tendon of a linear

actuator. The wear on the feeder is also an issue. If the feeder is severely worn, the surface of the feeder becomes uneven and the force applied to the tendon from the feeder becomes instable. Future work should quantitatively evaluate the durability of the tendon and the feeder.

### References

[1] S. Seok, C. D. Onal, K.-J. Cho, R. J. Wood, D. Rus, and S. Kim, "Meshworm: A Peristaltic Soft Robot With Antagonistic Nickel Titanium Coil Actuators," *IEEE/ASME Trans. Mechatronics*, vol. 18, no. 5, pp. 1485–1497, Oct. 2013.

[2] K. J. Kim and S. Tadokoro, *Electroactive Polymers for Robotic Applications*. Springer-Verlag London, 2007.

[3] S.-W. Kim, J.-S. Koh, J.-G. Lee, J. Ryu, M. Cho, and K.-J. Cho, "Flytrap-inspired robot using structurally integrated actuation based on bistability and a developable surface," *Bioinspir. Biomim.*, vol. 9, no. 3, p. 036004, Sep. 2014.

[4] R. F. Shepherd, F. Ilievski, W. Choi, S. A. Morin, A. A. Stokes, A. D. Mazzeo, X. Chen, M. Wang, and G. M. Whitesides, "Multigait soft robot," *Proc. Natl. Acad. Sci.*, vol. 108, no. 51, pp. 20400–20403, Nov. 2011.

[5] M. Calisti, M. Giorelli, G. Levy, B. Mazzolai, B. Hochner, C. Laschi, and P. Dario, "An octopus-bioinspired solution to movement and manipulation for soft robots," *Bioinspir. Biomim.*, vol. 6, no. 3, p. 036002, Sep. 2011.

[6] D. Sasaki, T. Noritsugu, M. Takaiwa, and H. Yamamoto, "Wearable power assist device for hand grasping using pneumatic artificial rubber muscle," in *13th IEEE International Workshop on Robot and Human Interactive Communication, 2004. ROMAN 2004*, 2004, pp. 655–660.

[7] J. Arata, K. Ohmoto, R. Gassert, O. Lambercy, H. Fujimoto, and I. Wada, "A new hand exoskeleton device for rehabilitation using a three-layered sliding spring mechanism," in *2013 IEEE International Conference on Robotics and Automation (ICRA)*, 2013, pp. 3902–3907.

[8] E. Obropta, D. N. Low, C. Link, B. Holschuh, E. Obropta, and D. Newman, "Low Spring Index NiTi Coil Actuators for Use in Active Compression Garments," *IEEE/ASME Trans. Mechatronics*, vol. 20, no. 3, pp. 1264–1277, 2015.

[9] A. T. Asbeck, S. M. M. De Rossi, K. G. Holt, and C. J. Walsh, "A biologically inspired soft exosuit for walking assistance," *Int. J. Rob. Res.*, vol. 34, no. 6, pp. 744–762, 2015.

[10] S. Lee, K. A. Landers, and H.-S. Park, "Development of a Biomimetic Hand Exotendon Device (BiomHED) for Restoration of Functional Hand Movement Post-Stroke," *IEEE Trans. Neural Syst. Rehabil. Eng.*, vol. 22, no. 4, pp. 886–898, Jul. 2014.

[11] Y.-L. Park, B. Chen, N. O. Pérez-Arancibia, D. Young, L. Stirling, R. J. Wood, E. C. Goldfield, and R. Nagpal, "Design and control of a bio-inspired soft wearable robotic device for ankle-foot rehabilitation," *Bioinspir. Biomim.*, vol. 9, no. 1, p. 016007, 2014.

[12] V. Bartenbach, K. Schmidt, M. Naef, D. Wyss, and R. Riner, "Concept of a soft exosuit for the support of leg function in rehabilitation," *IEEE Int. Conf. Rehabil. Robot.*, vol. 2015-September, pp. 125–130, 2015.

[13] H. In, B. B. Kang, M. Sin, and K. Cho, "Exo-Glove : Soft wearable robot for the hand using soft tendon routing system," *IEEE Robot. Autom.*, vol. 22, no. 4, pp. 97–105, 2015.

[14] A. T. Asbeck, K. Schmidt, I. Galiana, D. Wagner, and C. J. Walsh, "Multi-joint Soft Exosuit for Gait Assistance," *IEEE Int. Conf. Robot. Autom.*, pp. 6197–6204, 2015.

[15] Y. Mao and S. K. Agrawal, "Design of a cable-driven arm exoskeleton (CAREX) for neural rehabilitation," *IEEE Trans. Robot.*, vol. 28, no. 4, pp. 922–931, 2012.

[16] V. Chernyak, T. Flynn, J. O'Rourke, J. Morgan, A. Zalutsky, S. Chernova, S. S. Nestinger, and T. Padir, "The design and realization of a high mobility biomimetic quadrupedal robot," in *2012 IEEE/ASME International Conference on Mechatronics and Embedded Systems and Applications (MESA)*, 2012, pp. 93–98.

[17] Y. Ding, I. Galiana, A. Asbeck, B. Quinlivan, S. M. M. De Rossi, and C. Walsh, "Multi-joint actuation platform for lower extremity soft

exosuits," in *2014 IEEE International Conference on Robotics and Automation (ICRA)*, 2014, pp. 1327–1334.

[18] S. Crandall and T. Lardner, *An Introduction to the Mechanics of Solids: Second Edition with SI Units*, 2 edition. Boston: McGraw-Hill Science/Engineering/Math, 1999.

[19] THK, "Ball Screw THK General Catalog." THK, pp. 679–850, 2015.

[20] D. Tabor, "CV. The mechanism of rolling friction," *London, Edinburgh, Dublin Philos. Mag. J. Sci.*, vol. 43, no. 345, pp. 1055–1059, Jul. 1952.

[21] J. F. Archard and W. Hirst, "The Wear of Metals under Unlubricated Conditions," *Proc. R. Soc. A Math. Phys. Eng. Sci.*, vol. 236, no. 1206, pp. 397–410, Aug. 1956.

[22] A. Cardou, "Taut helical strand bending stiffness," *UFTscience*, 2006. [Online]. Available: [http://imechanica.org/files/Cardou\\_art\\_2006.pdf](http://imechanica.org/files/Cardou_art_2006.pdf). [Accessed: 24-Nov-2015].

[23] U. Jeong, H.-K. In, and K.-J. Cho, "Implementation of various control algorithms for hand rehabilitation exercise using wearable robotic hand," *Intell. Serv. Robot.*, vol. 6, no. 4, pp. 181–189, Sep. 2013.

[24] A. Peer and M. Buss, "A New Admittance-Type Haptic Interface for Bimanual Manipulations," *IEEE/ASME Trans. Mechatronics*, vol. 13, no. 4, pp. 416–428, Aug. 2008.

[25] L. E. Carlson, B. D. Veatch, and D. D. Frey, "Efficiency of Prosthetic Cable and Housing," *J. Prosthetics Orthot.*, vol. 7, no. 3, pp. 96–99, 1995.



**Hyunki In (S'09)** received the B.S. and Ph.D. degree in mechanical and aerospace engineering from Seoul National University, Seoul, Korea, in 2009 and 2015. He was a Postdoctoral Fellow with Biorobotics laboratory in Seoul National University, Seoul, Korea. He is currently working at convergence agricultural machinery R&D Group in Korea institute of industrial technology.



**Useok Jeong (S'10)** received the B.S. degree in mechanical and aerospace engineering from Seoul National University, Seoul, Korea, in 2010, where he is currently Ph. D candidate with BioRobotics Laboratory, department of mechanical and aerospace engineering. His research interests include rehabilitation robots, soft wearable robots, control of assistive devices, and dynamics modeling with control.



**Haemin Lee (S'13)** received the B.S. degree in mechanical and aerospace engineering from Seoul National University, Seoul, Korea, in 2013, where he is currently Ph. D candidate with BioRobotics Laboratory, department of mechanical and aerospace engineering. His research interests include assistive devices, rehabilitation robots, and tendon-driven mechanism



**Kyu-Jin Cho (M'08)** received the B.S and M.S. degrees from Seoul National University, Seoul, Korea, in 1998 and 2000, respectively, and the Ph.D. degree in mechanical engineering from the Massachusetts Institute of Technology, Cambridge, in 2007. He was a Postdoctoral Fellow with Harvard Micro-robotics Laboratory, Cambridge, until 2008. He is currently an Associate Professor of mechanical and aerospace engineering and the Director of the BioRobotics Laboratory, Seoul National University. His research interests include biologically inspired robotics, robotic systems using smart actuators, novel mechanisms using smart structures, and rehabilitation and assistive robotics.